The final publication is available at

http://doi.org/10.1016/j.mcm.2010.03.018

Additional Information

Moving mesh generation strategy solving an injector internal flow problem

Xandra Margot, Sergio Hoyas[1], Pablo Fajardo and Stavroula Patouna
CMT - Motores Térmicos
Universidad Politécnica de Valencia
Camino de Vera S/N, 46022 Valencia, Autor: Sergio Hoyas
e-mail: xmargot, serhocal, pabfape, stapa1@mot.upv.es

Abstract

The ability to handle complex geometries is an important part of transient calculations; therefore, the need for fully automatic mesh generation capable of dealing with general geometries is quite demanded. In this paper a specific approach to fully automatic three-dimensional mesh generation is presented. An approach of moving the generated mesh is also outlined. Particularly, the simulation of a diesel injector needle movement is sought. The movement of the needle in the moving meshes calculations based on injection rate experimental data and injection rate predicted data with steady state boundaries and geometry. The simulation performed with the commercial code STAR-CD version 4.06.

Keywords: Moving mesh method; Finite volume method, Diesel Injector

1. Introduction

In several situations it is convenient for the computational grid to follow moving boundaries. When fluid flow simulations involve changing geometry, the moving mesh options is an attractive alternative. Moving grid methods have been generally less developed and less well-known than the other adaptive techniques. In the past decade, there have been some efforts in understanding the theoretical backgrounds of the moving mesh methods [1, 2, 3, 4, 5, 6, 7]. The basic idea of moving mesh method is to construct a transformation from a logical fixed domain (computational domain) to the physical one. A fixed mesh is given on the logical domain, and the transformation is carried out by solving moving mesh partial differential equations or minimization problems for a functional mesh [8, 9, 10, 11] . However, the extension to transient problems does not seem simple.

---

[1] Corresponding author

Several mesh movement strategies are available: a) prescribed surface movement with automatic mesh morphing, b) explicit 3-D mesh movement via user functions or multiple mesh files, c) remeshing with topology change d) any combinations of the previous strategies. These strategies meet almost every conceivable mesh movement need. Various software give the possibility to automatically change the mesh by offering innovative dynamic mesh models where the user only required to set-up the initial mesh and specify the motion of the boundaries but little information is documented about the detailed procedure.

In diesel engines, the nozzle internal flow greatly affect the fuel atomization characteristics and so the subsequent engine combustion and exhaust emissions. The need of simulating the transient behavior and predict the real spray characteristics is of great importance. The transient nature of the flow is greatly affected by the needle movement. There are also studies referring to moving mesh studies of diesel injector needle but limited information is published about the mesh generation and moving grid methodology used to simulate the motion of the needle [12, 13, 14]. Moreover the needle movement is usually simulated considering simple linear equations. While, the present paper introduces a method of imposing the needle lift curve based on injection rate experimental data and injection rate results of calculations at fixed needle lifts.

The paper follows this outline: it starts with a mathematical description of the models implemented in the simulations. In section 3, the general methodology for the moving mesh generation and movement approach is presented. In section 4 the numerical case of the diesel injection simulation will be presented illustrating thus the method followed. Some conclusion remarks will be made in the last section.

2. Models description

Although the detailed mathematical documentation of the models can be found elsewhere [16], the numerical implementation of the models is highlighted in order to help the reader to better evaluate the methodology and the predicted results.

2.1. Mass and momentum conservation equations

The mass and momentum conservation equations are solved by STAR-CD using the Navier-Stokes equations in general non-steady coordinates [15]:

$$\frac{1}{\sqrt{g}}\frac{\partial \rho}{\partial t}\left(\sqrt{g}\,p\right)+\frac{\partial}{\partial x_j}\left(\rho \tilde{u}_j\right)= s_m \qquad\qquad , \text{Eq. 1}$$

$$\frac{1}{\sqrt{g}}\frac{\partial}{\partial t}\left(\sqrt{g}\,\rho u_i\right)+\frac{\partial}{\partial xj}\left(\rho \tilde{u}_j u_i - \tau_{ij}\right)= -\frac{\partial p}{\partial x_i}+ s_i \qquad , \text{Eq. 2}$$

Where t is time, x_i the Cartesian coordinate (i=1,2,3), u_i the absolute fluid velocity component in direction x_i, u_j the relative velocity ($u_j - u_{cj}$) between fluid and local (moving) coordinate frame that moves with velocity u_{cj}, p the piezometric pressure, ρ the density, t_{ij} stress tensor components, s_m the mass source, s_i the momentum source components and $\sqrt{g}$ is the determinant of the metric tensor.

2.2. Turbulence modeling

Additionally to the aforementioned conservation equations, the conventional two-equation k-ε model has been used to simulate the effects of turbulence. This model is a 2-equations model belonging to the Eddy Viscosity Models category (EVM). The transport equations for this model are as follows:

Turbulence kinetic energy equation

$$\frac{\partial}{\partial t}(\rho k)+\frac{\partial}{\partial x_j}\left[\rho u_j k - (\mu+\frac{\mu_t}{\sigma_k})\frac{\partial k}{\partial x_j}\right]= \mu_t(P+P_B) - \rho\varepsilon - \frac{2}{3}\left(\mu_t\frac{\partial u_i}{\partial x_i}+\rho k\right)\frac{\partial u_i}{\partial x_i}+\mu_t P_{NL} \quad \textbf{¡Error! Marcador no definido.}, \text{Eq. 3}$$

where

$$P \equiv S_{ij}\frac{\partial u_i}{\partial x_j} \qquad\qquad , \text{Eq. 4}$$

$$P_B \equiv -\frac{g_i}{\sigma_{h,t}}\frac{1}{\rho}\frac{\partial \rho}{\partial x_i} \qquad\qquad , \text{Eq. 5}$$

$$P_{NL} = -\frac{\rho}{\mu_t}\overline{u_i' u_j'}\frac{\partial u_i}{\partial x_j} - \left[P - \frac{2}{3}\left(\frac{\partial u_i}{\partial x_i}+\frac{\rho k}{\mu_t}\right)\frac{\partial u_i}{\partial x_i}\right] \quad , \text{Eq. 6}$$

P_{NL} = 0 for linear models, σ_k is the turbulent Prandtl number and μ_t the turbulent viscosity. The first term on the right-hand side of Eq.3 represents turbulent generation by shear and normal stresses and buoyancy forces, the second viscous dissipation, and the third amplification or attenuation due to compressibility effects. The last term accounts for the non-linear contributions.

Turbulence dissipation rate equation

$$\frac{\partial}{\partial t}(\rho\varepsilon) + \frac{\partial}{\partial x_j}\left[\rho u_j\varepsilon - \left(\mu + \frac{\mu_t}{\sigma_\varepsilon}\right)\frac{\partial\varepsilon}{\partial x_j}\right] =$$

$$C_{\varepsilon1}\frac{\varepsilon}{k}\left[\mu_t P - \frac{2}{3}\left(\mu_t\frac{\partial u_i}{\partial x_i} + \rho k\right)\frac{\partial u_i}{\partial x_i}\right] + C_{\varepsilon3}\frac{\varepsilon}{k}\mu_t P_B - C_{\varepsilon2}\rho\frac{\varepsilon^2}{k} \quad , \text{Eq. 7}$$

$$+ C_{\varepsilon4}\rho\varepsilon\frac{\partial u_i}{\partial x_i} + C_{\varepsilon1}\frac{\varepsilon}{k}\mu_t P_{NL}$$

where σ_ε is the turbulent Prandtl number and $C_{\varepsilon1}$, $C_{\varepsilon2}$, $C_{\varepsilon3}$ and $C_{\varepsilon4}$ are coefficients whose values kept as the defaults in the configuration of the model.

2.3. Cavitation modeling

In the current study, the commercial code STAR-CD is used for flow and cavitation prediction. The code offers the option of one cavitation model namely the Rayleigh model which was adopted in the current study [16]. The basic assumptions of this model are the following: Cavitation seed bubbles are present in the liquid and are homogeneously distributed and of equal size; the initial seed radius is one of the model parameters and must be specified by the user. The number of seed bubbles per unit volume of liquid is constant and is also a model parameter to be specified. All bubbles present in a control volume at any time are spherical and of the same size. Both liquid and vapour densities are constant. Other liquid and vapour component properties (such as molecular viscosity, specific heat capacity, thermal conductivity, etc.), as well as the saturation pressure, can be variable. The density ratio of vapour to liquid is small, $\ll$ 1. There is no slip between bubbles and liquid, i.e. vapour bubbles are treated as a component of the effective fluid. The transport of vapour is computed using Eq. 8.

$$\frac{\partial a_i}{\partial t} + \nabla(a_i u) = S a_i \quad \text{Eq. 8}$$

The source term describes the growth and collapse of vapour bubbles. The initial volume fraction of vapour is defined by the number of seed bubbles and their initial

radius (see Eq. 12). As bubbles move through the solution domain, their radius changes according to the local pressure. The rate of change of a bubble's radius along its path (the bubble growth velocity) is estimated using the Rayleigh equation:

$$\frac{dR}{dt} = sign(p_v - p)\sqrt{\frac{2|p_v - p|}{3\rho_1}} \qquad \text{Eq. 9}$$

where R is the bubble radius, p_v the saturation pressure and p the local pressure around the bubble. With the help of this equation an expression for the volumetric vapour source or sink at a given location in space is derived.

$$\sum_{i=1}^{Nc} a_i = 1 \qquad \text{Eq. 10}$$

The rate at which the vapour bubble grows when it passes a given location in the flow domain depends, according to the Eq. 9 only on the local pressure and not on its radius or the history of previous changes. This fact makes for an easy transition from a Lagranian to an Eulerian analysis. Following the assumption of a prescribed number n_o of spherical bubbles of radius R within a unit volume of liquid and the definition of volume fraction given by equation Eq. 11.

$$a_i = \frac{V_i}{V} \qquad \text{Eq. 11}$$

the vapour volume fraction can be expressed as

$$a_v = \frac{\left(4\pi R^3 / 3\right) n_o}{1 + \left(4\pi R^3 / 3\right) n_o} \qquad \text{Eq. 12.}$$

From the expression for the material derivative of a_v one arrives, after some re-arrangement and using the continuity equation for the effective fluid, to the expression for the source term in Eq. 8. This is of the following form:

$$Sa_v = \frac{4\pi R^2 n_o}{1 + \left(4\pi R^3 / 3\right) n_o} \frac{dR}{dt} \qquad \text{Eq. 13}$$

Substitution of Eq. 9 for the bubble growth rate leads to the final expression for the source term.

3. Methodology

3.1. Mesh generation

To apply the method proposed, the first step is to define the initial mesh (cut) which is the one that is not subject to motion. The initial mesh can be created according the needs of the problem using a mesh generation software and be stored in a file that will be later read with a macro. In this study the initial geometry was meshed by the automatic mesher of STAR-CCM+ Version 3.02.003. STAR-CCM+ contains different types of meshing models that can be used to generate a volume mesh starting from a suitably prepared surface mesh. As long as the initial mesh remains the same, extracting coordinate information from edge lines the desired geometry is achieved by defining vertices. These vertices will be subjected to motion and also will be used to generate the surface (patch) which maintains certain uniformity during mesh motion. The simplicity and reliability of this mesh generation approach together with the mesh movement method is demonstrated by the numerical example of a diesel injector case in three space dimensions in Section 3.

3.2. Equations of moving mesh operations

For this type of problem, an additional equation called the 'space conservation law' is solved for the moving coordinate velocity components (**Eq. 14**).

$$\frac{1}{\sqrt{g}}\frac{\partial \sqrt{g}}{\partial \tau} - \frac{\partial}{\partial x_t}\left(u_{cj}\right) = 0 \quad \text{Eq. 14}$$

This relates the change in cell volume to the cell-face velocity. The simultaneous satisfaction of the space conservation law and all other equations of fluid motion facilitates the general moving mesh operations performed. Mesh motion involving the 'arbitrary' (in reality, within distortion limits) motion of the cell vertices has been catered for by working from the outset with the general forms of the governing differential equations in an arbitrary moving coordinate frame. The development and solution of the discretised forms of these equations is straightforward within the finite volume framework, provided that appropriate measures are taken to ensure obedience to the so-called space conservation law [17].

3.3. Mesh movement

Mesh design in problems with a moving mesh and changing cell connectivity is dominated by the need to keep the dynamic parts of the grid simple so that they can be easily changed during the transient run. A set of grid-manipulation commands are supplied to be executed at each time step to specifying the vertex positions as function of time.

Before calculating with moving mesh, calculations with fixed needle calculations performed, i.e the geometry was fixed. Since the needle lift law in function of time is not known and could not be measured, the following technique was followed to extract it. Six calculations were performed, each at a different needle lift and the curve injection rate in function of needle lift was thus obtained. A correspondence between this curve and the experimentally measured injection rate yields then the needle lift law in function of time. (Fig. 1, a). The interpolated points between the curve injection rate in function of needle lift and the measured injection rate plotted and the slopes that found between them (Fig. 1, b) programmed in the calculations. The slopes were slightly rounded off (the lift law points vary slightly from the interpolated points) to facilitate the programming.
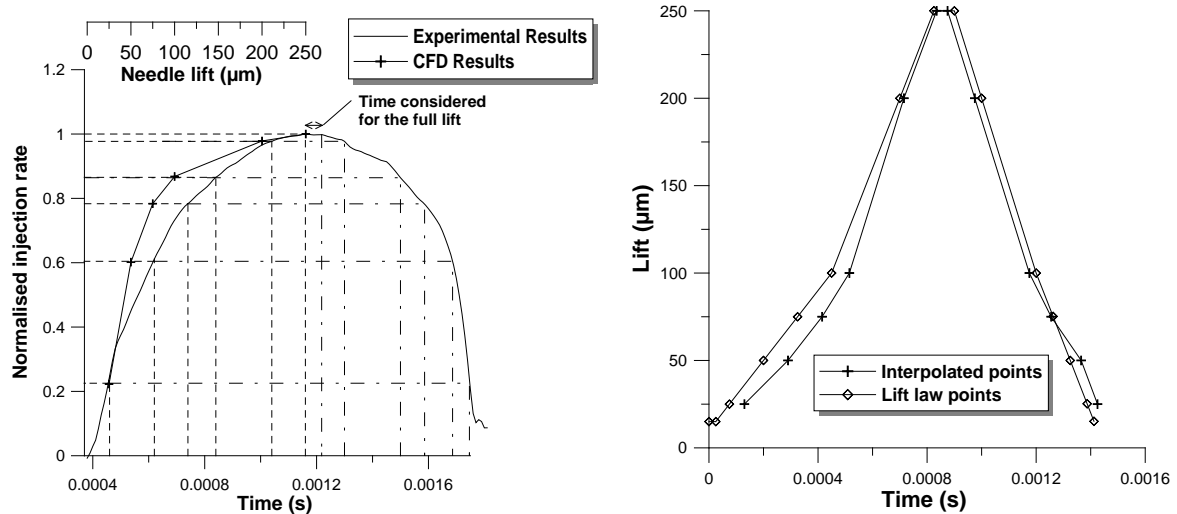

Fig. 1: a) Mass flow interpolation between experimental and computational results at fixed needle lifts b) Interpolated points and lift law considered for the calculations versus time.

Thus, the estimated velocity function of time for the needle lift opening and closing is used to move the needle in the transient calculations by the Eq. 15 which is valid for every slope of the lift curve.

$$lift = lift(t_0) + slope * (Time - t_0)$$ Eq. 15

where $lift(t_0 = 0) = 0$ and t_0 the time at which each slope begins.

With the appropriate slope the solution needle displacement procedure can be illustrated by the following flowchart:

1) Start calculation at time 0

2) Calculate displacement A(0) , where A(0) the needle lift

3) Delete all cells

4) Import the initial mesh

5) According the A(0) calculate the new coordinates on the moving part that define the new surface

6) Create the patch surface

7) Extrude the patch creating the domain (meshed). The number of cells are defined via user commands

8) Delete the patch

9) Merge the double vertices

10) Make the connectivity between the fixed and moving part

11) Calculate

12) Repeat the step 2-11 until reaching a determinate time value

4. Example

In this problem, the vertices that are subject to motion are those that define the bottom of the needle while the moving area is the annulus formed between the needle and the needle seat. In Fig. 2 the needle at full lift and at low lift is seen, illustrating thus the annulus that is created from its movement which is the flow pass. The bottom part on the injector with 10 µm needle lift considered as initial mesh that is not subject to motion in this study (see Fig. 3, a). A low needle lift value has to be considered as the solver cannot handle with meshes whose size is zero. The cell size of the initial mesh used is that of the fixed needle meshes, so as to have the same size cell in both fixed and moving needle mesh calculations. In the simulation a 60 degree sector of the injector geometry considered.
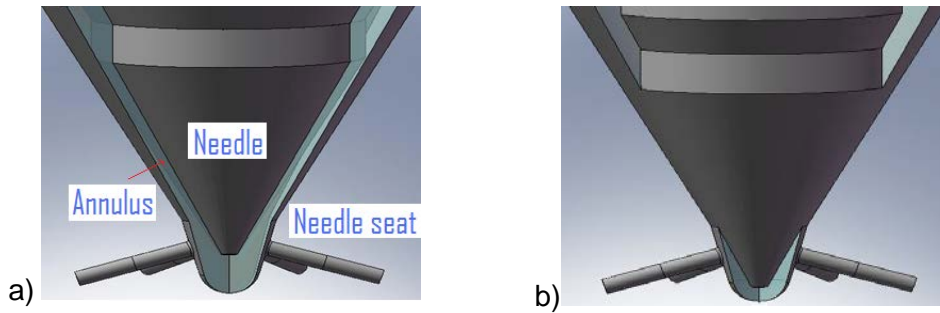
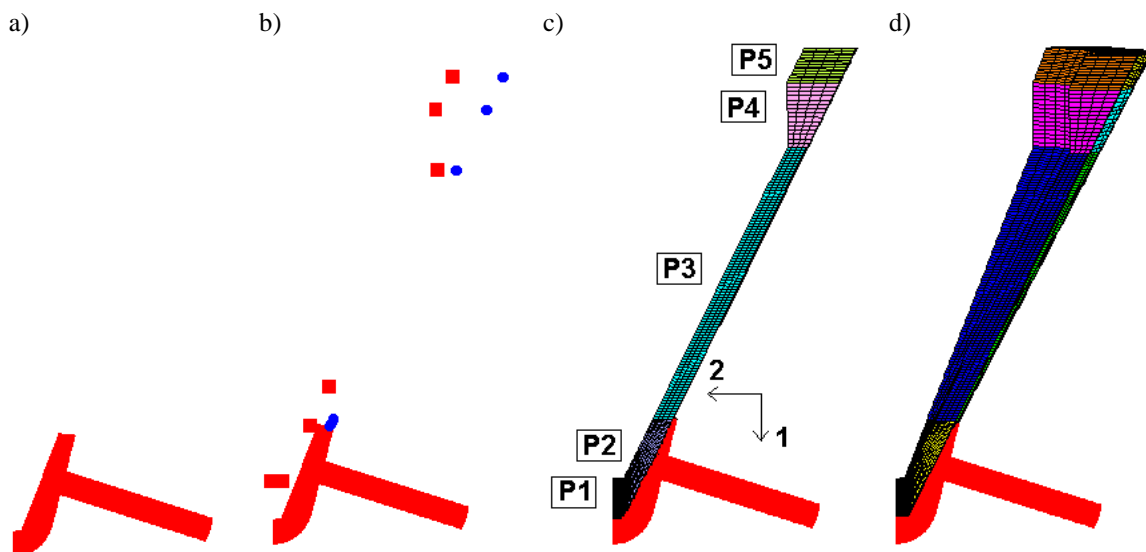Fig. 2: a) Needle at full lift, b) Needle at a low lift

Fig. 3. a) Initial mesh at 10 μm lift needle lift, b) vertices defining the contour, in squares the vertices subject to motion c) patches defined for mesh generation, d) full needle lift mesh after extrusion

Once the initial geometry meshed, the vertices that define the contour of the geometry at full lift (250 μm) have to be specified (Fig. 3, b). These vertices then enable us to create patches that represent the solution domain geometry (5 patches created, see Fig. 3, c). The patches are defined in terms of characteristics points (vertices that are not subject to motion) and derived points (vertices that are subject to motion) and then extrudes along a specified direction and coordinate system in order to obtain the mesh corresponding to the full needle lift (Fig. 3, d). The extrusion consists in defining the number of cells that the mesh will have in each direction (Fig. 4). The patch can be extruded to create a three dimensional mesh block once the user decides the number and distribution of the cells depending on the geometrical complexity of the model. The geometry and the mesh are now fully defined but due to the fact that patches are considered by STAR-CD as walls, they have to be removed, as well as the double vertices created during the patch.

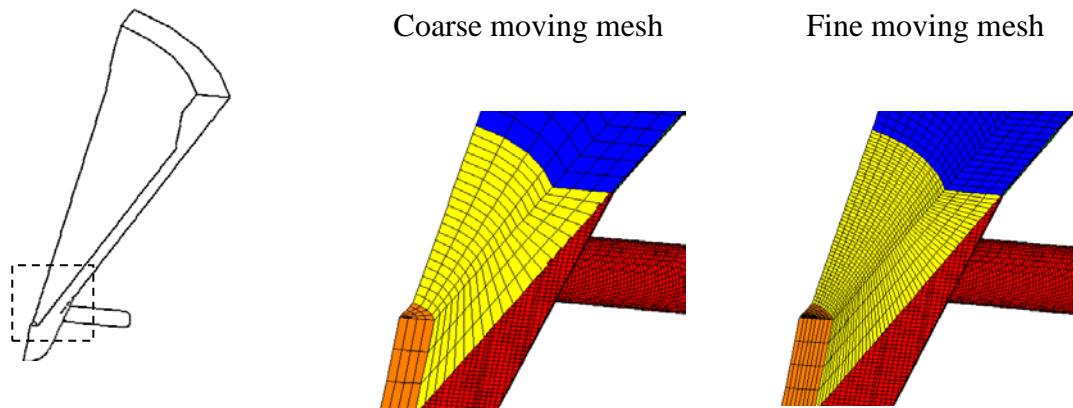Coarse moving mesh   Fine moving mesh

Fig. 4. Meshes of the moving part occurred by the extrude facility.

generation. The meshes of the annulus between the needle and the needle seat stretch and shrink with the needle movement.

The final step is to define the connectivity between the fixed and the moving part of the mesh by creating couples of cells at the interfaces. The mesh is now complete and ready to use for calculation.

Two directions of the coordinate system used in order to move the mesh in this study. The patch P1 is moved following the direction number 2 defined in Fig. 3, b. The distance considered for the displacement is the one directly calculated in the user subroutine, since this patch follows the lift of the needle. The other patches, P2, P3, P4, and P5 are moved following the direction number 1. In order to follow the real needle valve opening the displacement of these patches is equal to half of the calculated displacement of the needle (P1). This is allowable due to the conventional geometry of the injector considered. The nozzle seating forms angle of 30o with the axis of the nozzle so the displacement of these patches assumes the value of (needle displacement * sin 30o). It is thus possible to have the real geometry displacement, and also to keep the mesh aspect constant, only the cell size changes. The other possibility would have been to move all the patches following the direction number 2, using the displacement calculated as for P1. However, the former strategy was preferred in order to avoid the deformation of the mesh during needle valve closing. This deformation generated negative volumes for the cells on the interface between the fixed part and the moving one.

The simulation was realized for different operating conditions and particularly the phenomenon of cavitation was studied. Fig. 5 shows the results of the CFD injection rate compared to the experimental injection rate, both normalized with the maximum values of each rate. The small differences observed between the experimental and measured mass flow rates are due to the constraints of the interpolation made on the lift law. Results of the diesel injector flow behavior of this study are documented in [18].
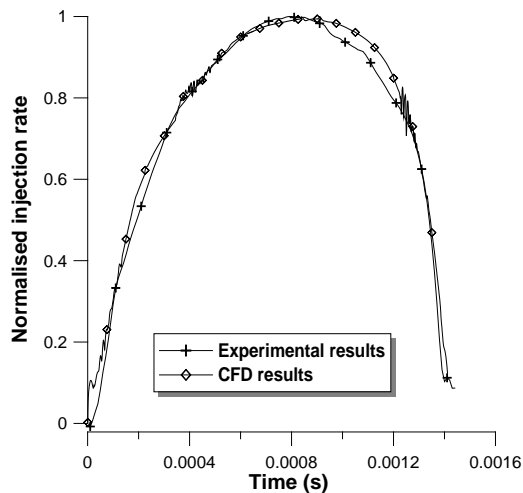

Fig. 5: Comparison between CFD and experimental injected mass flow rate.

5. Conclusions

In this paper, we have presented a simple moving mesh strategy for solving a multi-phase flow in a diesel injector nozzle. The approach for the needle movement in this study required an interpolation between the experimental results and the results with calculations at fixed needle lifts. The moving mesh computation was satisfactory in terms not only of accuracy but also efficiency.

Acknowledgements

[1]   J.H. Smith and A.M. Stuart, Analysis of continuous moving mesh equations, 1996, Technical report, SCCM Program, Stanford University, Stanford, CA

[2]   J.H. Smith, Analysis of moving mesh methods for dissipative partial differential equations, Ph.D. thesis, Stanford University, Dept. Computer Science, 1996

[3]   Y. Qiu, D.M. Sloan, and T. Tang, Numerical solution of a singularly perturbed two-point
boundary value problem using equidistribution: analysis of convergence, J. Comput. Appl. Math. 106 (2000), 121–143

[4]   T. Linß, Uniform pointwise convergence of finite difference schemes using grid equidistribution, Computing 66 (2001), 27–39

[5]   G. Beckett and J.A. Mackenzie, Convergence analysis of finite-difference approximations on equidistributed grids to a singularly perturbed boundary value problem, Appl. Numer. Math.35 (2000), 209–131.

[6]   T. Dupont and Y. Liu, Symmetric error estimates for moving mesh Galerkin methods for
advection-diffusion equations, SIAM J. Numer. Anal. 40 (2002), 914–927

[7]   Y. Liu, R.E. Bank, T.F. Dupont, S. Garcia, and R.F. Santos, Symmetric error estimates for moving mesh mixed methods for advection-diffusion equations, SIAM J. Numer. Anal. 40 (2003), 2270–2291

[8]   M.J. Baines, M.E. Hubbard and P.K. Jimack, A Lagrangian moving finite element method incorporating monitor functions. In: Y.Y. Lu, W.W. Sun and T. Tang, Editors, Advances in Scientific Computing and Applications, Science Press, Beijings/New York (2004), pp. 32–44.

[9]   W.M. Cao, W.Z. Huang and R.D. Russell, An r-adaptive finite element method based upon moving mesh PDEs, J. Comput. Phys. 149 (1999), pp. 221–244.

[10]   W.Z. Huang and R.D. Russell, Moving mesh strategy based on a gradient flow equation for two-dimensional problems, SIAM J. Sci. Comput. 20 (1999), pp. 998–1015

[11]   R. Li, T. Tang and P. Zhang, A moving mesh finite element algorithm for singular problems in two and three space dimensions, J. Comput. Phys. 177 (2002), pp. 365–393

[12]   U. Michels., C. Krüger , G. König , M. Blessing , V. Schwarz , G. P. Merker Analysis of the Influence of the Injection Strategy on Cavitating Nozzle Flow, Spray Formation and combustion in a Heavy Duty Truck engine, Effects on Spray and Mixture Formation, Thermo-and fluid dynamic processes in Diesel Engines Conference (THIESEL), 2004.

[13]   B. Argueyrolles, D. Passerel, D. Maligne, Influence of the nozzle Geometry on Diesel Injector Internal Flow: a Computational Approach, THIESEL 2004 Conference on Thermo-and fluid dynamics processes in Diesel Engines, Valencia, Spain, 2004.

[14]   M.Gavaises, D. Papoulias, E. Gianadakkis, A. Andriotis, N. Mitroglou and A. Theodorakakos, Comparison of cavitation formation and development in Diesel VCO nozzles with cylindrical and converging tapered holes, Thermo-and fluid dynamic processes in Diesel Engines Conference (THIESEL), 2008.

[15]   Warsi, Z.V.A. 1981. 'Conservation form of the Navier-Stokes equations in general nonsteady coordinates', AIAA Journal, 19, pp. 240-242.

[16]   STAR-CD Methodology, version 4.06, CD adapco, 2008.

[17]   Demirdzic, I., and Peric, M. 1988. 'Space conservation law in finite volume calculations of fluid flow', Int. J. Numer. Methods in Fluids, 8, pp. 1037–1050.

[18]   F. Payri, X. Margot, S. Patouna, F. Ravet, M. Funk, A CFD study of the effect of the needle movement on the cavitation pattern of Diesel Injectors, to be published in Conference on Society of Automotive Engineers International (SAE) Paper, 2009-24-0025, 2009.